Room-temperature ferromagnetism in Mn-implanted amorphous Ge

L. Ottaviano, A. Continenza, and G. Profeta
Dipartimento di Fisica, Università degli studi dell'Aquila, Via Vetoio 10, I-67100 L'Aquila, Italy

G. Impellizzeri and A. Irrera
CNR-IMM MATIS and Dipartimento di Fisica e Astronomia, Università di Catania, Via S. Sofia 64, I-95123 Catania, Italy

R. Gunnella
CNISM, Università di Camerino, Via Madonna delle Carceri, I-62032 Camerino (MC), Italy

O. Kazakova
National Physical Laboratory, Hampton Road, Teddington, Middlesex TW11 0LW, United Kingdom
(Received 26 April 2010; revised manuscript received 8 July 2010; published 20 April 2011)

A 2×10^{16} Mn^+/cm^2 100 keV ion implantation at liquid-nitrogen temperature onto Ge(100) surfaces produces a perfect Mn dilution into a completely amorphized Ge layer (155 nm thickness and 4% average Mn concentration) as directly demonstrated by Mn K-edge x-ray absorption spectroscopy. Superconducting quantum interference device (SQUID) investigations demonstrate that this diluted magnetic semiconductor system exhibits ferromagnetism up to room temperature. The magnetic response is explained within the model of percolation of bound polarons. Once the Mn fluence is doubled during the implantation, SQUID measurements clearly point to formation of Mn-Mn dimers and phase separation of Mn into Mn-rich amorphous clusters. First-principles calculations on Mn-doped amorphous Ge give a rationale to the experiments at the lowest fluence showing that disorder in the amorphous phase with the distortion of the Ge tetrahedra plays a crucial role, favoring the Mn substitutional inclusion and, correspondingly, enhancing the magnetic response of the system.

DOI: 10.1103/PhysRevB.83.134426 PACS number(s): 75.70.−i, 61.05.cj, 68.37.Hk, 71.15.Mb

I. INTRODUCTION

Spintronics, i.e., spin transport electronics, is a revolutionary concept of the last two decades that already has had a tremendous impact on everyday life and technology with the discovery of giant magnetoresistance, which has led to an explosive development of magnetic storage devices.[1] When compared to such glorious success, the route toward the realization of another class of materials (whose importance is largely believed to be pivotal in the development of future spintronic devices), namely, diluted magnetic semiconductors (DMSs), has not been very straightforward. No consensus has yet been reached on a technologically appealing procedure to reliably and reproducibly obtain a room temperature (RT) DMS, where spin and charge can be simultaneously controlled.[2] Indeed, with the notable exception of metal oxide semiconductors[3] and GaN,[4] despite tremendous efforts, the achievement of ferromagnetism at room temperature (and above) for those semiconductors that are by far the most widely used and of technological appeal (i.e., GaAs for groups III–V and Si and Ge for group IV semiconductors) has not been reported so far for the bulk phase. On the other hand the interest in Mn doping of Ge systems has very recently witnessed a strong revival.[5–10]

In a DMS, high Curie temperatures T_C (namely, above RT) can be typically achieved by increasing the concentration of the magnetic dopants (typically Mn) in the semiconductor. The required concentration values are well beyond the extremely low solubility limit of the magnetic dopants in any host semiconductor matrix.[11] To resolve this problem, the use of far from equilibrium fabrication techniques such as molecular beam epitaxy (MBE) is needed. In this case, usually, only by carefully playing with the growth parameters (such as substrate temperature, or adopting the "delta-doping" strategy[12]) can the presence of precipitates be minimized. For example, focusing the attention on the Mn-Ge system, the typical occurrence of the secondary phase is in the form of amorphous Mn-rich cluster[13], or even the more stable Mn_5Ge_3 (Refs. 14 and 15) or Mn_5Ge_2 and $Mn_{11}Ge_8$ (Ref. 16) precipitates. Of particular disadvantage is the tendency of Mn to form dimers (antiferromagnetically coupled) in the host crystalline matrix.[17,18] These occurrences altogether hamper the raising of the T_C with an increase of the dopant concentration. Moreover, in the presence of precipitates in a host DMS matrix, the whole system can exhibit fascinating phenomena typical of a "meta-material" such as the occurrence of magnetically induced low-temperature metal insulator transitions,[19] or cluster-related memory effects.[20] On the other hand, from the point of view of spintronics applications, which require the fabrication of homogeneous materials at the nanoscale, the presence of precipitates can indeed significantly deteriorate the potential appeal of such real world materials.

An alternative approach to MBE, proposed in the latest years is ion implantation. Our group has extensively considered this strategy in the case of Mn doping of Ge (see Ref. 14 and references therein). Nonetheless, also with ion implantation, even if almost perfect dilution can be achieved in a subsurface implanted layer,[17] we still observed either unavoidable phase precipitation [for implantation substrate temperatures above 240°C (Ref. 17)] or the occurrence of Ge swelling below 200°C (Ref. 21) with the formation of a highly radiation damaged layer of porous sponge-like amorphous Ge usually on top of a compact amorphous Ge-Mn layer.[22] Thus, all the evidence accumulated so far indicate that there is little

or no room for a significant stable and homogeneous dilution of Mn in crystalline Ge.

Evidently other routes have to be explored. Already in Ref. 22 we envisaged the possibility of obtaining a single-phase ferromagnetic response from the implanted compact amorphized layer. Others[23] have speculated on the expectation to significantly lift the Mn solubility in the host semiconductor matrix (and accordingly the T_C of the DMS) by diluting Mn in amorphized Ge (a-Ge). Magnetic doping of a-Ge has been already explored by Choe,[23] Paek,[24] and Yu[25] (by means of rf sputtering, or thermal co-evaporation on substrates kept at room temperature) but with controversial results and little insight into their properties from a fundamental point of view. For instance, a rationale was not proposed to explain why magnetic doping of a-Ge should be more viable in terms of dilution and more effective in terms of the magnetic response.

Ion implantation of Ge can be the best suitable technique for Mn doping in an amorphous semiconductor matrix. It has been extensively studied that swelling typically occurs only in a well-defined range of the substrate temperatures T_{gr} during ion implantation [$T_{gr} \simeq 300$–500 K (Ref. 26)]. On the other hand, swelling is almost independent of the ion species, ion energy, and ion fluence. It is important to note that when the substrate temperature during the implantation is kept well below room temperature (i.e., $T_{gr} = 77$ K), the swelling is not observed anymore, and the implantation produces only a compact layer of amorphized Ge. This was directly demonstrated by Holland[26] and Appleton[27] with transmission electron microscopy (TEM) images and electron diffraction patterns in the case of Bi ion implantation on Ge(100) kept at liquid-nitrogen (LN) temperature. Similarly, Stritzker[28] demonstrated that, almost regardless of the ion fluence, swelling does not occur at T_{gr} below 190 K. Thus, with the aim of obtaining a homogeneous Mn dilution into amorphous Ge, we prepared our system via ion implantation of Mn in Ge(100) at $T_{gr} = 77$ K, and performed a thorough and complementary theoretical and experimental investigation of its properties.

In this paper we report two main observations: (i) For a 2×10^{16} Mn/cm^2 fluence, LN ion implantation produces amorphization; Mn is perfectly diluted in a-Ge; the system exhibits a single-phase ferromagnetic response at least up to room temperature; and the structural disorder effectively lifts the Mn solubility and improves the magnetic response of such a DMS. (ii) When the Mn concentration is doubled (4×10^{16} Mn/cm^2 fluence), the magnetic response is significantly weaker, and phase separation into Mn-rich clusters occurs.

II. EXPERIMENTAL AND CALCULATION DETAILS

The (001)-oriented *n*-type Czochralski (Cz) Ge wafers, with a nominal resistivity 10^{-2}–10^{-3} Ω cm, were implanted with 100 keV Mn^+ ions with two fluences of 2×10^{16} and 4×10^{16} ions/cm^2, respectively. During the implantation the substrate was set with the (001) axis forming an angle of 7° with respect to the impinging beam direction to avoid channeling. From SRIM Monte Carlo simulation,[29] the expected projected range R_p (i.e., the depth of maximum concentration) for Mn ions at the chosen beam energy is ≃55 nm, and the end of the implantation range is situated at ≃160 nm. The substrate temperature during the implantation was checked by means of a thermocouple (faced to the wafer back side) with an accuracy of 2°C. For implantation at the LN temperature the substrate was kept in thermal equilibrium with a liquid-nitrogen cold finger. The Mn concentration distribution profile for Mn ion implanted Ge at identical fluences can be found in Ref. 30; the implantation produces a quasi-Gaussian Mn concentration profile in the 160 nm thick implanted film with Mn peak concentrations, respectively, of 0.08 and 0.16 at 50 nm depth from the implanted surface (Fig. 1 in Ref. 30).

Tapping-mode atomic force microscopy (AFM) measurements were performed *ex situ* in air with a Digital Dimension D5000 instrument equipped with a Nanoscope IV controller, using a Si cantilever (300 kHz resonance frequency). Scanning electron microscopy (SEM) images were taken with a LEO 1503 apparatus equipped with a field effect gun. X-ray absorption (XAS) measurements were performed at the BM8 beamline in the European Synchrotron Radiation Facility (ESRF) in conventional fluorescence mode by an array of 13 elements of a Ge solid-state detector.[31] The Mn K-edge was measured around the absorption white line (6550 eV) by means of a Si(111) monochromator and passing bandwidth of 1/10000.

XAS spectra of reference standards like Mn_5Ge_3, MnO, and Mn_2O_3 were also measured. All XAS measurements were performed at room temperature, and a metal reference sample was used to calibrate the photon beam energy during the measurement sessions. Theoretical XAS spectra were calculated within a full multiple scattering (MS) potential formalism (extensively illustrated in Ref. 32) choosing various structural cluster models. Magnetic properties of as prepared Ge-Mn thin films were studied using superconducting quantum interference device (SQUID) magnetometry (Quantum Design). Measurements were performed in a dc regime at temperatures between 1.8 and 300 K and in fields up to 10 kOe with the magnetic field applied in the film plane.

Standard precautions for working with low-moment samples were undertaken, in particular, only ceramic tools were used for sample handling. The identical experimental routine was applied to the reference sample (nonimplanted Ge from the same batch of wafers used for the implantation). The magnetization of the Ge-Mn thin film was calculated by normalization of the experimental magnetic moment by the volume of the magnetic material, assuming a film thickness of $t = 150$ nm (from SRIM and SEM evidence). First-principles VASP (Vienna *ab initio* simulation package) calculations[33] were carried out for Mn impurities substituted in the ST12 structure which is generally acknowledged as a good model of disordered tetrahedrally coordinated Ge.[34] To calculate the magnetic interaction between Mn impurities, a 2×2×2 unit cell (96 atoms) was used, placing two Mn atoms into two inequivalent structural sites (at increasing distances in different calculations).

III. SEM, AFM, AND STRUCTURAL XAS ANALYSIS

Figure 1 shows cross-sectional SEM images of 100 keV Mn^+ implanted Ge(100) at 170°C (top panel), and at LN substrate temperature (bottom panel). The top panel image is shown for comparison. The electron beam to the Ge(100)

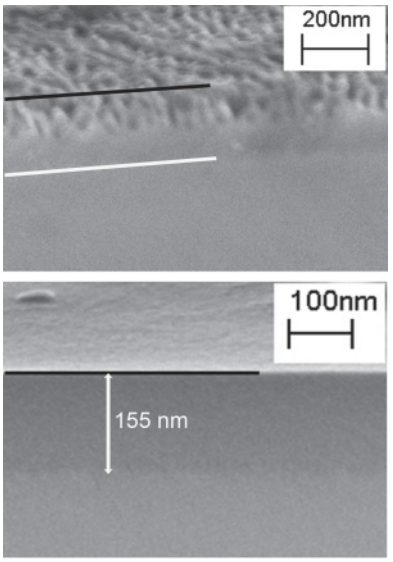

FIG. 1. Cross-sectional SEM images of 100 keV 2×10^{16} Mn ions/cm^2 irradiated Ge(100) surfaces at 170°C (top panel) and LN substrate temperature (bottom panel).

surface normal angle during acquisition of the images was 70°. In the two panels two horizontal black lines are drawn as a guide for the eye to mark the edge between the Ge(100) surface (upper part of the images) and the cross-sectional wall. The top panel of the figure shows the effects of Ge swelling upon ion irradiation (substrate at 170°C). As a guide to the eye, a white line in the image marks the depth where a clear SEM contrast change is observed. The black-white line separation is roughly consistent with the SRIM-predicted depth of the implantation layer; accordingly we assign the implanted layer to the region in between the dark and white lines. The topmost implanted layer shows a sponge-like morphology with a random network of columnar Ge nanostructures and voids of 10–20 nm size. This is the so-called swelled Ge layer: amorphous and containing oxidized Mn.[22]

We observed swelling whenever the Ge substrate temperature was kept below (about) 200°C, and down to RT during implantation.[22] This phenomenon is likely due to the coalescence of vacancies into large voids[35] but its quantitative understanding is beyond the scope of the present investigation. Instead, for the purposes of our work, it is interesting to note that the implanted layer underneath the swelled one is amorphous. This was directly verified by us with TEM in Ref. 22 for RT Mn implantation onto Ge(100).

Once the substrate temperature is decreased (down to LN), then swelling is not observed anymore (see the bottom panel of Fig. 1). The implanted sample surface does not show voids and a sponge-like structure. The surface morphology of such LN ion implanted samples was investigated with AFM. Figure 2 does not show the three-dimensional morphology typical of swelled Ge (like in Ref. 21), the surface is flat with a root-mean-square value of the roughness equal to 2.2 Å. It is also interesting to note that the samples (implanted at LN) show absence of swelling already after a visual inspection, having a mirror-like surface [definitely different from the black color of oxidized swelled implanted Ge (Ref. 26)]. Very interestingly, in the SEM cross sectional view there is a well-defined

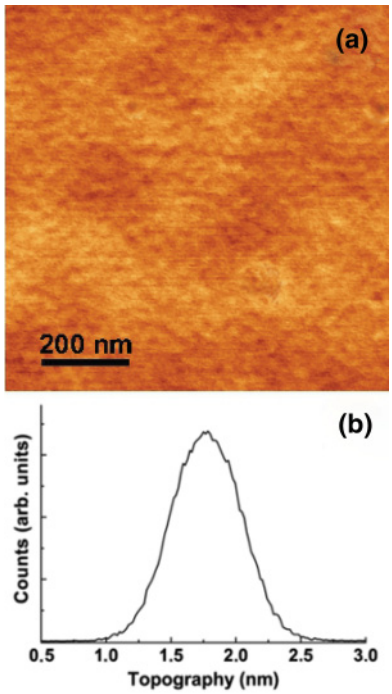

FIG. 2. (Color online) Top: AFM image of the surface of a Ge(100) sample after ion implantation of 100 keV, 2×10^{16} Mn (LN substrate temperature). Bottom: corresponding height distribution with rms roughness of 2.2 Å.

region of darker contrast whose width (155 ± 5 nm) is in excellent agreement with the amorphous layer thickness (160 nm) determined with a SRIM simulation (2×10^{16} Mn at 100 keV) once a displaced per atom (DPA) number of 0.1 [typical for implantation in a Ge matrix at LN (Ref. 36)] is assumed. The occurrence of such sharp contrast is not observed in TEM images for Mn implantation temperatures well above the swelling regime (at 300°C) where dynamical annealing occurs and the Ge matrix remains compact and crystalline.[37] This contrast, which does not show a modulation in the 155 nm region below the edge, cannot be assigned to a "chemical contrast" caused by the Mn inclusion, because Mn has a pseudo-Gaussian profile of concentration in the implanted layer.[22] Rather, consistent with SRIM, we assign this contrast as due to a "phase" contrast between the implanted amorphous Ge layer and the crystalline Ge beneath. The formation of a nonswelled amorphous Ge layer by ion irradiation, once the substrate is kept at LN, has been already demonstrated with TEM and Rutherford back-scattering measurements by Holland *et al.*[26] More recently Impellizzeri *et al.*[36] studying the self-implantation of Ge with Ge at LN at equivalent implantation fluences, demonstrated (by means of Rutherford back scattering and profilometry) that the implanted layer of Ge at LN temperature is amorphous with a density decrease of about 2.0%. Though such a direct measurement was not performed in our case, a similar density decrease effect can be more than likely assumed for the LN implantation of Mn in Ge. We thus assign our observation of a uniform darker contrast of the LN implanted Ge to its being amorphous and less dense, and accordingly to its generating a lower electron yield under the primary electron beam of the SEM system.

The structural characterization of the Mn-Ge implanted samples, like the one shown in Fig. 1, has been carried out by means of XAS. It is worth stressing that this technique is extremely suitable to investigating the local chemical and structural environment of magnetic dopants in DMS systems. For instance, very recently, Soo *et al*. preformed a similar SQUID-XAS combined investigation on magnetically doped (Mn and Cr) amorphous silicon.[38] As pointed out in Refs. 17 and 39 for Mn-Ge alloys (fabricated either with ion implantation or MBE) Mn K-edge XAS experiments, allow (i) observation of the occurrence of phase precipitation in the DMS alloy of Mn into Mn-rich phases (like Mn_5Ge_3 crystalline or amorphous clusters), (ii) evidence of the occurrence of formation of Mn-Mn dimers, (iii) discrimination between interstitial and substitutional Mn in a Ge host, and (iv) quantitative determination the type of order or disorder (crystalline or amorphous) of the local (very first few nm around the Mn atom) Ge host matrix surrounding the Mn atom. The above information is of utmost importance in determining the degree of Mn dilution in the Ge matrix.

The Mn K-edge XAS spectrum of the Mn-Ge system under investigation is reported in the upper panel of Fig. 3 (diamonds). A number of very solid points can be raised before discussing a quantitative analysis of the data. First, compared to other ion implanted Mn-Ge systems with identical Mn implantation fluence[17] the XAS features are really faint. This occurrence can be straightforwardly assigned to the high degree of disorder in this specific system pointing to the assignment of an amorphous phase. Second, this XAS spectrum is very similar to the one (the RT Mn-implanted sample reported in Ref. 39) obtained from XAS experiments on another Mn-Ge system whose amorphous nature has been evidenced with TEM.[22] This occurrence is verified once the swelled amorphous Ge layer of the RT implanted alloy is removed (Fig. 3 in Ref. 22) and the subsurface disordered Mn-implanted amorphous Ge layer is measured with XAS. Third, our XAS experiments allow us to rule out with high confidence the presence of interstitial occupation of Mn. Interstitials are very prone to diffusion and cluster formation upon annealing of the samples.[39] This typically produces notable changes in the XAS spectra of Mn-Ge systems prior to and after annealing. Noteworthily, instead, the XAS spectrum of Fig. 3 remains totally unchanged upon annealing the sample even up to 400°C.

Another occurrence that can be ruled out by analyzing this spectrum is the absence of any detectable trace of Mn-rich precipitates either in the amorphous or crystalline phase; this occurrence (according to Refs. 17 and 39) would lead to very specific peaks in the XAS spectrum at the energies of 6553, 6563, 6575, and 6596 eV, which are definitely absent in the spectrum of Fig. 3.

Thus the above arguments point to the absence of Mn interstitials and Mn atoms in Mn-rich Mn-Ge clusters. More detailed structural information can be determined by the fitting analysis of the extended x-ray absorption fine structure (EXAFS) $\chi(k)$ spectrum reported in the inset of the lower panel of Fig. 3. The solid line in the $\chi(k) * k^2$ is the fitting line of the experimental data (dots). The fitting curve is calculated once considering just a single shell of 4 ± 0.1 first Ge neighbors at a distance of 2.51(2) Å. The variance σ^2 of

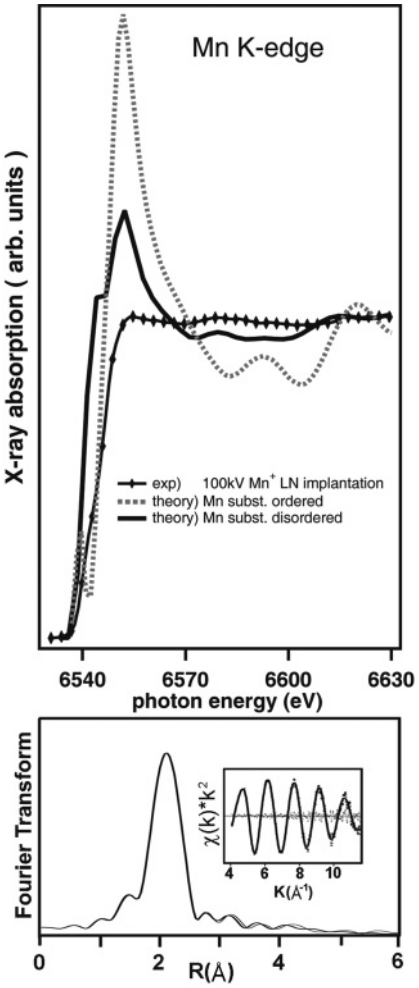

FIG. 3. Mn K-edge XAS absorption data for Mn-Ge LN implanted. Top panel: The ordered (dashes) and the disordered (solid) MS theory of the XAS are compared with the LN implanted experimental spectrum (diamonds). Lower panel: Fourier transform of the EXAFS signal (inset in the panel) from the experimental spectrum of the top panel.

such distance is 0.008 Å^2 comparable to the one determined for other Mn-Ge alloys.[39] Noteworthily, the fitting analysis allows us to exclude any detectable presence of Mn dimers. All the above information leads to the conclusion that the Mn is in a substitutional site. To answer the question, "Is the host Ge matrix crystalline or disordered ?" we then performed full multiple scattering (MS) calculations for a cluster of Mn in a crystalline diamond substitutional site (dashed curve in Fig. 3) or, on the other hand, with an Mn atom hosted substitutionally in a distorted ST12 Ge structure[34] (solid curve in Fig. 3). The calculated XAS spectra have been adjusted to the experimental one by normalization of the jump of the cross section between 6535 and 6625 eV. The ST12 phase, described later on in the section of first-principles calculations, is still a crystalline one, but in terms of nearest-neighbor pair distribution function, it very nicely mimics (on the short-range order, which is the one probed by XAS) germanium in the amorphous phase.[34] Direct comparison of the two MS calculated spectra with the experimental one, clearly shows that a better agreement is observed when passing from the crystalline diamond MS

spectrum to the one of the ST12 phase, where local distortion of the tetrahedra is taken into account. To further support this point we also note that the Fourier transform (FT) of Fig. 3 (lower panel) is very similar to the FT of amorphized Ge (EXAFS experiments) obtained by LN implantation of Ge into Ge by Ridgeway *et al.*[40] Thus this evidence also indicates, from a microscopic point of view, that the host Ge matrix in our Mn-Ge system is amorphous.

A final but very important remark concerning this structural analysis is on the determined value of the Mn-Ge nearest-neighbor distance 2.51 Å. This is the typical Mn-Ge coordination distance for Mn diluted in a host Ge matrix.[39] This value is about 2% larger than the Ge-Ge coordination distance in crystalline Ge (c-Ge), and this mismatch is a sign of the difficulty of Mn dilution in the Ge matrix. On the other hand, once Ge is amorphized (by Ge ion implantation), as reported by Ridgeway *et al.*,[40] there is a clear trend (with the ion fluence) to the increase of the Ge-Ge nearest-neighbor distance toward 2.47 Å. This indicates the presence in the Ge matrix of point defects, i.e., threefold (T3) and fivefold (T5) coordinated atoms. Noteworthily, such defects are characterized by a nearest-neighbor distance of 2.52 and 2.57 Å, respectively.[41] Accordingly we suggest that Mn atoms are most likely accommodated in T3 and T5 sites. The fact that the average number of nearest neighbors as determined by the EXAFS analysis of Fig. 3 is about 4.0 is because the five-fold coordinated Mn's likely occur with the same probability as the three-fold ones, as in Ref. 40. Finally we note that the direct observation in our case of a 2% strain of the lattice parameter, together with a similar finding for the Ge-Ge distance in the very similarly prepared a-Ge system of Ridgeway,[40] are perfectly in line with the determination of a 2.0% density decrease of Ge implanted Ge at LN by Impellizzeri *et al.*[36]

IV. MAGNETIC RESPONSE: SQUID MEASUREMENTS

The summary of magnetization measurements is shown in Fig. 4. Diamagnetic background originating from a Ge substrate and a plastic straw used for the samples mounting was subtracted from all experimental results. The field dependence of the magnetization, the $M(H)$ curve, demonstrates a clear hysteretic behavior in the whole studied temperature range, $T = 5$–293 K [Fig. 4(a)]. Even at room temperature, the $M(H)$ dependence is characterized by a distinctive coercive field, $H_c = 120$ Oe, and saturation at $H_{\rm sat} = 2$ kOe [Fig. 4(a) inset]. As temperature decreases to $T = 50$ K, the overall shape of the hysteresis curve remains unaltered. In this temperature range, the saturation magnetization is on the order of 0.45–0.50 emu/cm^3. Opening of the hysteresis loop and their saturation in the moderate magnetic field suggest a ferromagnetic type of ordering in the system at $T \leqslant 300$ K. However, the observed ferromagnetic properties are relatively weak, as indicated by the low saturation moment. As temperature decreases, the saturation magnetization increases rapidly and reaches 1 emu/cm^3 at $T = 5$ K. The shape of the hysteresis notably changes and the saturation shifts toward higher magnetic fields as the temperature decreases. From this saturation value, the thickness of the implanted layer, and by knowing the Mn fluence, we estimate $\approx 0.08\ \mu_B$/Mn, in line with an anomalously low value observed also for Mn-doped amorphous silicon[42] and with recent results obtained for ion implanted Mn-Ge by Zhou *et al.*[9] It should be noted, that the hysteretic behavior was never observed in the reference sample [unimplanted Ge(100)], where the $M(H)$ dependence remained linear.

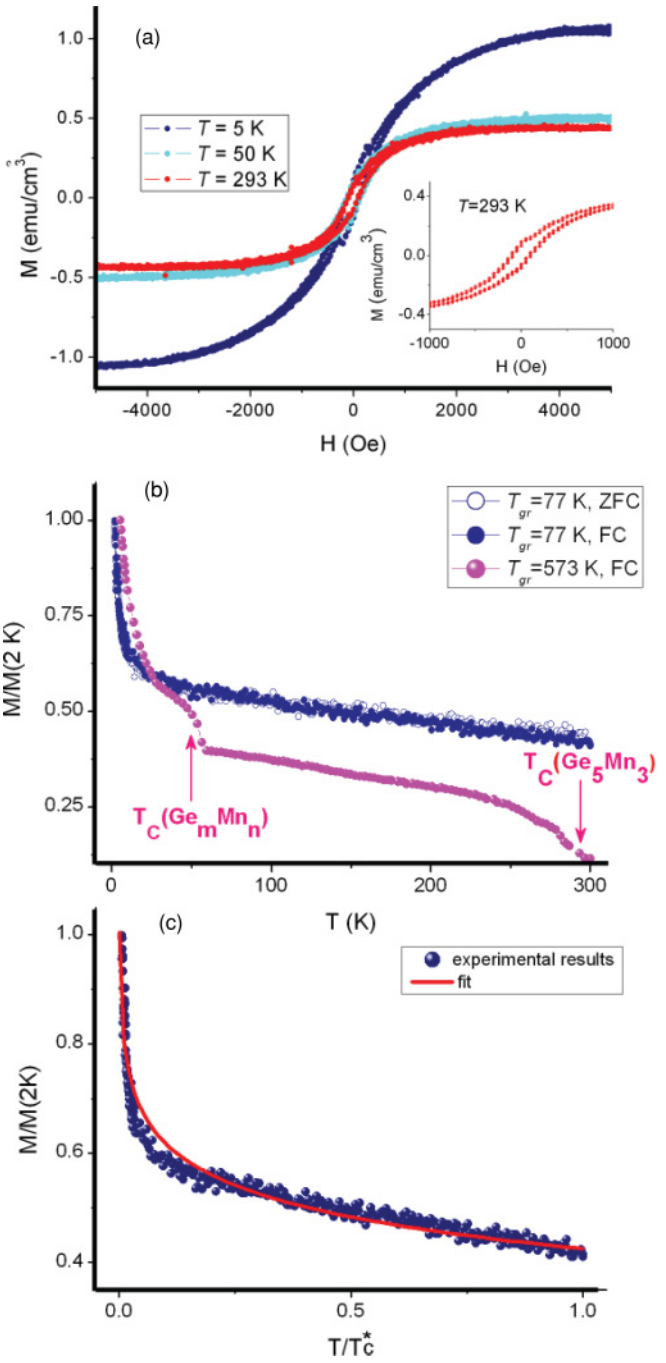

FIG. 4. (Color online) Magnetization measurements of the LN Mn-implanted Ge: (a) field and (b) temperature dependences of magnetization. In (b) magnetization was measured after field cooling and zero-field cooling at $H = 100$ Oe. The magnetization of a Ge-Mn sample implanted at $T = 573$ K is shown in (b) for comparison. (c) Temperature dependence of magnetization in normalized coordinates. The solid line is an approximation by Eq. (1) with the fitting parameter $a_B^3 n_h = 2.5\times10^{-3}$.

Figure 4(b) shows temperature dependences of the magnetization, M vs T, as measured in the warming cycle after either field cooling (FC) or zero-field cooling (ZFC) of the sample at $H = 100$ Oe. Both curves have a well-pronounced concave shape where the magnetization gradually decreases with temperature. It should be stressed that we do not observe any pronounced transition temperatures in the whole investigated temperature range, which could denote presence of a magnetically inhomogeneous phase or clusters of various nature. The FC and ZFC curves coincide in the whole temperature range, which signifies the reversibility of the field-induced changes and absence of the blocking temperature typical for the para- or super-paramagnetic systems. Another interesting feature is an absence of a sharp step at 290–295 K, which is typical for ferromagnetic transition in metallic Mn_5Ge_3 precipitates. This observation is consistent with the XAS results and rules out the presence of this extremely undesirable, but unfortunately very common metallic phase in other Ge-Mn systems (see, e.g., Refs. 43 and 44). For comparison, we plot the $M(T)$ dependence for a similar Ge-Mn sample implanted at $T = 573$ K [Fig. 4(b)]. The curve clearly demonstrates the occurrence of an inhomogeneous magnetic structure, consisting of Mn_5Ge_3 precipitates, amorphous Ge_nMn_m clusters and diluted Mn^{2+} ions. Each subsystem is characterized by its own transition temperature.[43] Further, we discuss the magnetic properties of the present a-Ge-Mn film within the percolation model[45] using assumptions of a strong disorder in the system and the fact that the indirect exchange between magnetic centers (Mn^{2+} ions) is carried out by localized charge carriers (holes in the case of Ge-Mn). In the case of an MBE grown Mn-Ge DMS system, this model has been adopted by Li *et al.*[46] The exchange interaction between localized holes and magnetic ions leads to formation of magnetic polarons (quasiparticles consisting of a localized and polarized hole and a number of surrounding magnetic ions). Using a formalism developed in Ref. 45 (the Kaminski and Das Sarma model), the temperature dependence of magnetization can be written as

$$M(T)/M_{2K} \propto 0.86 + \left(a_B^3 n_h\right)^{1/3} \ln(T_C^*/T), \qquad (1)$$

where M_{2K} is the magnetization at $T = 2$ K, a_B is the decay length of the hole's wave function, n_h is the hole concentration.[47] Thus, the shape of the magnetization curve is determined only by the dimensionless fitting parameter $a_B^3 n_h$. The experimental results were fitted using Eq. (1), see Fig. 4(c). A close correlation between the fit and the experimental data indicates a percolation nature of the ferromagnetism in the Ge-Mn thin film. The parameter $a_B^3 n_h = 2.5\times\ 10^{-3}$ obtained from the fit is significantly less than unity, which also points to the percolation mechanism of the ferromagnetic ordering and is associated with a strong localization of holes in the amorphous system.

Of particular interest is the comparison of the fitting parameter $a_B^3 n_h$ determined in this work with values of other DMS systems where the magnetic response is also within the frame of the percolation model.[44,48] In particular, it was demonstrated[44] that once the contribution of Mn-rich precipitates is subtracted, this model explains quite well the magnetic response of the Mn properly diluted in a crystalline Ge matrix, giving $a_B^3 n_h = 1.4\times10^{-2}$. On the other hand, the same percolation model holds for Cr-doped amorphous silicon, as demonstrated by Yao,[48] and in that case $a_B^3 n_h = 2.7\times10^{-5}$. The three values span almost three orders of magnitude, where a smaller value generally corresponds to a stronger carrier localization.

From the observed trend in the above $a_B^3 n_h$ values we extrapolate the effectiveness of the magnetic dopant dilution in substitutional tetrahedrally coordinated sites of the semiconductor matrix and, accordingly, the concentration of holes n_h. To this aim, particularly enlightening is the comparison between the a-Ge (this work) and the c-Ge Mn-diluted system.[44] In both cases, an identical Mn fluence was used. In the case when the Ge matrix is crystalline (c-Ge), despite a well-pronounced phase precipitation into Mn-rich clusters, a very significant fraction of Mn atoms was diluted in c-Ge substitutional sites.[17] On the other hand, in the present case all the Mn atoms are "diluted," but as discussed above (EXAFS results), they are very likely preferentially accommodated in defective T3 and T5 sites. Thus, such "defect trapped" Mn ions do not increase the hole concentration in the system. In

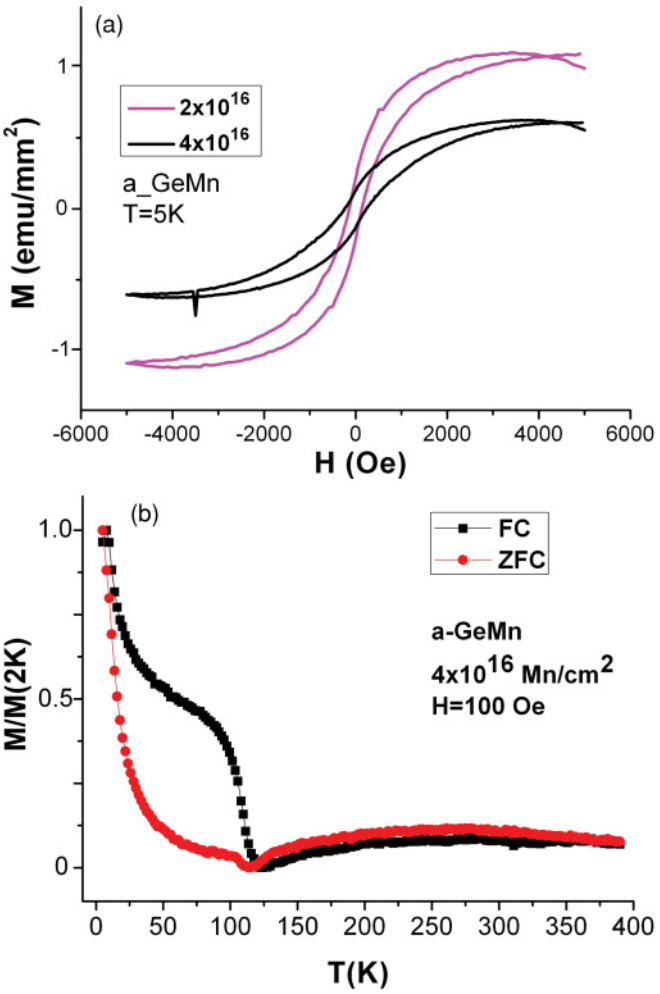

FIG. 5. (Color online) Magnetization measurements of LN Mn-implanted Ge for a 4×10^{16} Mn ions/cm^2 fluence: (a) field and (b) FC (ZFC) [black (red or gray) plots] temperature dependences of magnetization. In (a) the magnetization for the 2×10^{16} Mn ions/cm^2 fluence [purple or gray line] is reported for comparison.

line with this, the $a_B^3 n_h$ value is lower by almost an order of magnitude in a-Ge than in c-Ge. Finally, in the Cr a-Si system, a real dilution is definitely more difficult than in Ge,[49] and expectedly a very little fraction of the magnetic impurities contribute to holes, the $a_B^3 n_h$ parameter further drops two orders of magnitude.

Thus, our EXAFS results show that Mn dopants are incorporated in amorphous Ge without forming detectable Mn-Mn dimers and, therefore, exclude the possibility of a dominant direct exchange interaction between magnetic ions. The magnetic measurements also clearly demonstrate the absence of any detectable secondary phase and prove FM-type of ordering at $T \leqslant 300$ K. The observed magnetic properties can be satisfactorily described within the bound magnetic polaron model.

The above illustrated model is not valid any longer once the Mn concentration is doubled. We observe in Fig. 5(a) that the saturation magnetization is reduced by almost a factor of 2 (1.8, i.e., $\approx$0.045 μ_B/Mn). This occurrence can only be assigned to significant formation of Mn-Mn dimers, which are antiferromagnetically coupled and do not contribute to the overall magnetic response of the alloy. We estimate that, with doubling the Mn fluence, almost 50% of the Mn atoms, which could be magnetically active at lower fluence, are quenched by dimer formation. Furthermore, the $M(T)$ behavior of the Mn-implanted alloy at higher fluence significantly deviates from the pure "percolation" model [Fig. 5(b)]. In agreement with similar results reported recently[9,10] for Mn ion implanted Ge at a comparable fluence, the $M(T)$ curve shows a feature clearly noticeable in the 60–70 K temperature range that is always ascribed to phase precipitation of Mn into Mn-rich amorphous clusters (see Refs. 9 and 10 and references therein). This observation places an upper limit on the Mn concentration where perfect Mn dilution and a magnetic response solely due to percolation can be realized.

V. FIRST-PRINCIPLES CALCULATIONS

Different theoretical approaches have been proposed to describe the structural and electronic properties of amorphous semiconductor systems.[8,50,51] The most sophisticated ones use both molecular dynamics (MD) and density functional theory (DFT) calculations taking into account large (i.e., at least 64 atoms) supercells subsequently "melted" and "quenched" in the simulation.[8,51] The amorphization strategies via MD are substantially based on a seminal paper proposed in Ref. 52. Moreover, the approach can be simpler, by calculating within DFT, the structural and electronic properties of crystalline systems with reduced symmetry that locally mimic the structure of the real amorphous systems. In the case of a-Ge such a "simpler" structure is the ST12 phase.[34] This phase is a weakly ordered crystal, which turns out to be a very good compromise between structural likelihood and computational efforts to model a-Ge.[50] It has 12 atoms per unit cell and a space group with few symmetry operations.[53] Unlike diamond, the ST12 crystalline network exhibits seven- and five-fold atom rings and a fairly broad distribution of configurations of bonds on neighbors atoms, similar to a-Ge.[34] Simulations of a-Ge with such a distorted crystal phase model allow one to grasp most of the important properties of the real a-Ge system

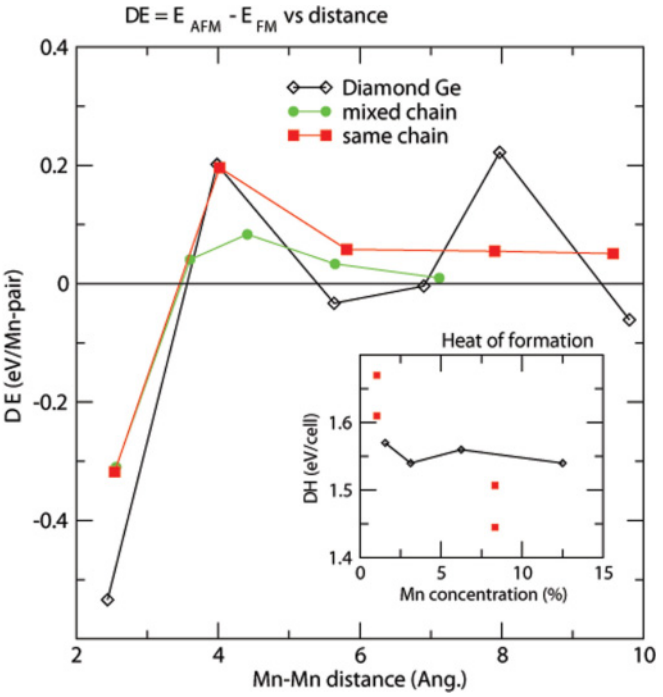

FIG. 6. (Color online) Magnetic interaction energy (eV/Mn-pairs) between two substitutional Mn atoms in the diamond (open symbols) and a-Ge phase (filled symbols). The inset shows the heat of formation of a substitutional Mn impurity as a function of Mn concentrations for diamond (open symbols) and ST12 Ge (filled symbols).

like its optical and electronic properties.[54,55] Our choice, thus, was to carry out first-principles calculations using as a model structure the ST12 phase.[34] The reasons for this choice are (i) the system is simpler than computer-generated amorphous systems, but still retains many important and fundamental structural properties of true a-Ge, (ii) most importantly, there is a very good fit of the local structural ST12 environment with the one of our a-Ge system (see Fig. 3), and (iii) finally, though comparison of MD simulations from subsequently melted and quenched structures is realistic for some experiments (like the a-Ge preparation in Ref. 8) it is far from obvious that the Ge amorphous structure obtained by ion implantation is consistent with the one obtained in MD simulations. In addition, as will be shown in the following, in terms of local magnetic moment the results obtained with our model calculation are quantitatively in agreement with those obtained using more sophisticated and computationally demanding approaches.[8]

The strength of the magnetic interaction between nearby Mn's, is related to the total energy difference between mutually antialigned (antiferromagnetic, AFM) and aligned (ferromagnetic, FM) spin directions on the Mn sites. This quantity is shown on Fig. 6 as a function of the distance between the two interacting Mn atoms and compared with the case of the Ge-diamond lattice. The peculiar ST12 structure allows for different possible substitutional sites depending on whether the Mn site lies along a chain of symmetry equivalent atoms (squares) or if it is connected to symmetry-nonequivalent sites (circles). While the symmetry of the diamond lattice imposes strongly directional magnetic interactions [favored

along the (110) axis], the same is no longer true for the more isotropic ST12 structure which (i) keeps the same total magnetic moment ($3\mu_B$) as in the diamond structure[56] in agreement with what was obtained, in the average, using more complex simulations for this same system in Ref. 8, (ii) shows AFM interaction between nearest-neighbor Mn atoms about 30% less, (iii) exhibits a monotonic and almost constant FM interaction at larger Mn distances, (iv) does not show strong anisotropy in the magnetic interaction (as expected in an amorphous-like compound), and (v) as a difference with the diamond structure—where a Ruderman-Kittel-Kasuya-Yosida (RKKY)-like interaction has been invoked—the magnetic coupling is always ferromagnetic at all distances larger than the nearest neighbor. Finally, as shown in the inset of Fig. 6 the heat of formation at Mn concentrations close to experiment (a few %) is quite lower if the Ge-host matrix is ST12 rather than diamond. This finding, together with the results obtained for the magnetic interactions between Mn's, suggests that an amorphous environment might favor incorporation of substitutional Mn impurity and possibly results in a stronger ferromagnetic interaction with respect to a perfect diamond-crystalline coordination. More details regarding the calculations together with a more complete discussion of the results can be found in Ref. 56. Finally, we argue that the discrepancy between the calculated magnetic moment per Mn atom with the value experimentally observed (in this work and also in similarly prepared systems[8]) has to be ascribed to the presence in the real a-Ge system of nonmagnetically active three- and five-fold Mn coordinated substitution atoms (as discussed in the previous section), which are difficult to be taken into account in the ST12 structure or in other more sophisticated calculations reported in the literature.[8]

VI. CONCLUSIONS

In conclusion, in this work we report a thorough experimental and theoretical investigation of the structural and magnetic properties of a manganese-doped amorphous germanium. The system has been fabricated by Mn ion implantation (2×10^{16} Mn^+/cm^2 fluence) onto crystalline Ge. The structural environment of the Mn impurities has been carefully investigated by Mn K-edge XAS, and, within the uncertainty of the method, the experimental evidences clearly point to (i) absence of Mn dimers, (ii) absence of Mn-rich precipitates in the form of clusters either crystalline or amorphous (as otherwise typically observed for attempts of Mn dilution in crystalline Ge), and (iii) absence of interstitial Mn atoms. Moreover, the EXAFS analysis clearly points to a model of distorted tetrahedra (amorphous Ge) where Mn impurities are substitutional with an average number of nearest Ge neighbors of 4 (± 0.1). The Mn atoms are accommodated in defective T3 and T5 sites not useful for lifting the magnetic response of the system. In line with this, SQUID measurements show a weak magnetic response (≈ 0.08 μ_B/Mn) which, on the other hand, notably persists with a ferromagnetic behavior (opening of the hysteresis loop) up to room temperature. The magnetic response is explained in terms of the bound magnetic polaron model. Finally, first-principles calculations demonstrate the higher solubility of Mn in an amorphous-like (ST12) structure of Ge and that, at variance with the crystalline Ge case, the coupling of the Mn atoms is always ferromagnetic. When the Mn fluence is doubled (to 4×10^{16} Mn^+/cm^2), the system loses its peculiar features of pure dilution. SQUID magnetometry results point at Mn dimer formation and precipitation of Mn into amorphous Mn-rich clusters.

ACKNOWLEDGMENTS

This work was partly funded by the UK BIS under project 114503 and EU FP7 NanoSpin. L.O. acknowledges also financial support from the Erasmus Placement program.

[1] P. Grünberg, R. Schreiber, Y. Pang, M. B. Brodsky, and H. Sowers, Phys. Rev. Lett. **57**, 2442 (1986).
[2] H. Ohno, Science **281**, 951 (1998).
[3] Y. Matsumoto, M. Murakami, T. Shono, T. Hasegawa, T. Fukumura, M. Kawasaki, P. Ahmet, T. Chikyow, S.-Ya Koshihara, and H. Koinuma, Science **291**, 854 (2001).
[4] A. C. Mofor, A. El-Shaer, A. Bakin, A. Waag, H. Ahlers, U. Siegner, S. Sievers, M. Albrecht, W. Schoch, N. Izyumskaya, and V. Avrutin, Appl. Phys. Lett. **87**, 62501 (2005).
[5] F. Xiu, Y. Wang, J. Kim, A. Hong, J. Tang, A. P. Jacob, J. Zou, and K. L. Wang, Nat. Mater. **9**, 337 (2010).
[6] I.-S. Yu, M. Jamet, T. Devillers, A. Barski, P. Bayle-Guillemaud, C. Beigné, J. Rothman, V. Baltz, and J. Cibert, Phys. Rev. B **82**, 035308 (2010).
[7] A. Jain, M. Jamet, A. Barski, T. Devillers, C. Prret, P. Bayle-Gullemaud, S. Gambardelli, V. Maurel, and G. Desfonds, Appl. Phys. Lett. **97**, 202502 (2010).
[8] Li Zeng, J. X. Cao, E. Helgren, J. Karel, E. Arenholz, L. Ouyang, D. J. Smith, R. Q. Wu, and F. Hellman, Phys. Rev. B **82**, 165202 (2010).
[9] S. Zhou, D. Bürger, W. Skorupa, P. Oesterlin, M. Helm, and H. Schimdt, Appl. Phys. Lett. **96**, 202105 (2010).
[10] S. Zhou, D. Bürger, A. Mücklich, C. Baumgart, W. Skorupa, C. Timm, P. Oesterlin, M. Helm, and H. Schimdt, Phys. Rev. B **81**, 165204 (2010).
[11] T. Dietl, H. Ohno, F. Matsukura, J. Cibert, and D. Ferrand, Science **287**, 1019 (2000).
[12] K. Yanagisawa, S. Takeuchia, H. Yoshitakea, K. Onomitsua, and Y. Horikoshia, J. Cryst. Growth **301-302**, 634 (2007).
[13] S. Sugahara, K. L. Lee, S. Yada, and M. Tanaka, Jpn. J. Appl. Phys. **44**, L1426 (2005).
[14] L. Ottaviano, M. Passacantando, A. Verna, P. Parisse, S. Picozzi, G. Impellizzeri, and F. Priolo, Phys. Status Solidi A **204**, 136 (2007).
[15] R. Gunnella, L. Morresi, N. Pinto, R. Murri, L. Ottaviano, M. Passacantando, F. D'Orazio, and F. Lucari, Surf. Sci. **577**, 22 (2005).
[16] Y. Wang, J. Zou, Z. Zhao, X. Han, X. Zhou, and K. L. Wang, Appl. Phys. Lett. **92**, 101913 (2008).
[17] L. Ottaviano, M. Passacantando, A. Verna, R. Gunnella, E. Principi, A. Di Cicco, G. Impellizzeri, and F. Priolo, J. Appl. Phys. **100**, 063528 (2006).

[18]F. D'Orazio, F. Lucari, S. Santucci, P. Picozzi, A. Verna, M. Passacantando, N. Pinto, L. Morresi, R. Gunnella, and R. Murri, J. Magn. Magn. Mater. **262**, 158 (2003).
[19]O. Riss, A. Gerber, I. Ya. Korenblit, A. Suslov, M. Passacantando, and L. Ottaviano, Phys. Rev. B **79**, 241202R (2009).
[20]S. Zhou, A. Shalimov, K. Potzger, N. M. Jeutter, C. Baehtz, M. Helm, J. Fassbender, and H. Schimdt, Appl. Phys. Lett. **95**, 192505 (2009).
[21]L. Ottaviano, A. Verna, V. Grossi, P. Parisse, S. Piperno, M. Passacantando, G. Impellizzeri, and F. Priolo, Surf. Sci. **601**, 2623 (2007).
[22]A. Verna, L. Ottaviano, M. Passacantando, S. Santucci, P. Picozzi, F. D'Orazio, F. Lucari, M. De Biase, R. Gunnella, M. Berti, A. Gasparotto, G. Impellizzeri, and F. Priolo, Phys. Rev. B **74**, 085204 (2006).
[23]G. Choe, A. P. Valanju, and R. M. Walser, IEEE Trans. Magn. **32**, 4538 (1996).
[24]W. B. Paek, J. Kim, and S. H. Lim, Phys. Status Solidi B **241**, 1521 (2004).
[25]S. S. Yu, T. T. L. Anh, Y. E. Ihm, D. Kim, H. Kim, S. K. Hong, S. Oh, C. S. Kim, H. J. Lee, and B. C. Woo, Curr. Appl. Phys. **6**, 545 (2006).
[26]O. W. Holland, B. R. Appleton, and J. Narayan, J. Appl. Phys. **54**, 2295 (1983).
[27]B. R. Appleton, O. W. Holland, J. Narayan, O. E. Schow III, J. S. Williams, K. T. Short, and E. Lawson, Appl. Phys. Lett. **41**, 711 (1982).
[28]B. Stritzker, R. G. Elliman, and J. Zou, Nucl. Instrum. Methods Phys. Res. B **175**, 193 (2001).
[29]J. F. Ziegler, J. P. Biersack, and U. Littmark, *The Stopping and Range of Ions in Solids* (Pergamon, New York, 1985).
[30]L. Ottaviano, M. Passacantando, S. Picozzi, A. Continenza, R. Gunnella, A. Verna, G. Bihlmayer, G. Impellizzeri, and F. Priolo, Appl. Phys. Lett. **88**, 061907 (2006).
[31]F. dAcapito, S. Colonna, S. Pascarelli, G. Antonioli, A. Balerna, A. Bazzini, F. Boscherini, F. Campolungo, G. Chini, G. Dalba, G. I. Davoli, P. Fornasini, R. Graziola, G. Licheri, C. Meneghini, F. Rocca, L. Sangiorgio, V. Sciarra, V. Tullio, and S. Mobilio, ESRF Newslett. **30**, 42 (1998).
[32]D. Sebilleau, R. Gunnella, Z.-Y. Wu, S. D. Matteo, and C. R. Natoli, J. Phys. Condens. Matter **18**, R175 (2006).
[33]G. Kresse and J. Furthmüller, Phys. Rev. B **54**, 11169 (1996); Comput. Mater. Sci. **6**, 1 (1996).
[34]A. Mujica and R. J. Needs, Phys. Rev. B **48**, 17010 (1993).
[35]T. Janssens, C. Huyghebaert, D. Vanhaeren, G. Winderickx, A. Satta, M. Meuris, and W. Vandervorst, J. Vac. Sci. Technol. B **24**, 510 (2006).
[36]G. Impellizzeri (unpublished).
[37]M. Passacantando, L. Ottaviano, F. D'Orazio, F. Lucari, M. De Biase, G. Impellizzeri, and F. Priolo, Phys. Rev. B **73**, 195207 (2006).
[38]Y. L. Soo, J. H. Yao, C. S. Wang, S. L. Chang, C. A. Hsieh, J. F. Lee, and T. S. Chin, Phys. Rev. B **81**, 104104 (2010).
[39]R. Gunnella, L. Morresi, N. Pinto, A. Di Cicco, L. Ottaviano, M. Passacantando, A. Verna, G. Impellizzeri, A. Irrera, and F. DAcapito, J. Phys. Condens. Matter **22**, 216006 (2010).
[40]M. C. Ridgeway, C. J. Glover, K. M. Yu, G. J. Foran, C. Clerc, J. L. Hansen, and A. Nylandsted Larsen, Phys. Rev. B **61**, 12586 (2000).
[41]G. Kresse and J. Hafner, Phys. Rev. B **49**, 14251 (1994).
[42]Li Zeng, E. Helgren, M. Rahimi, F. Hellman, R. Islam, B. J. Wilkens, R. J. Culbertson, and D. J. Smith, Phys. Rev. B **77**, 073306 (2008).
[43]R. Morgunov, M. Farle, M. Passacantando, L. Ottaviano, and O. Kazakova, Phys. Rev. B **78**, 045206 (2008).
[44]R. B. Morgunov, A. I. Dmitriev, and O. L. Kazakova, Phys. Rev. B **80**, 085205 (2009).
[45]A. Kaminski and S. Das Sarma, Phys. Rev. Lett. **88**, 247202 (2002).
[46]A. P. Li, J. F. Wendelken, J. Shen, L. C. Feldman, J. R. Thompson, and H. H. Weitering, Phys. Rev. B **72**, 195205 (2005).
[47]As a first approximation in the fit we used $T_C^* = 300$ K, based on the fact that it was the largest measurement temperature in the experiment and the hysteresis loop still remains open. In reality we expect that T_C^* is somewhat larger than 300 K.
[48]J.-H. Yao, H.-H. Lin, and T.-S. Chin, Appl. Phys. Lett. **92**, 242501 (2008).
[49]ÊH. Okamoto, *Bulletin of Alloy Phase Diagrams* (American Society for Metals, Metals Park, OH, 1992), Vol. 3, p. 2.
[50]L. Pizzagalli, G. Galli, J. E. Klepeis, and F. Gygi, Phys. Rev. B **63**, 165324 (2001).
[51]N. C. Cooper, C. M. Goringe, and D. R. McKenzie, Comput. Mater. Sci. **17**, 1 (2000).
[52]I. Stich, R. Car, and M. Parrinello, Phys. Rev. B **44**, 11092 (1991).
[53]The space group of ST12, P43212, has eight symmetry operations, to compare with the 192 symmetry operations of the space group Fd3m of the cubic diamond structure.
[54]J. D. Joannopoulos and M. L. Cohen, Phys. Rev. B **7**, 2644 (1973).
[55]I. B. Ortenburger and D. Henderson, Phys. Rev. Lett. **30**, 1047 (1973).
[56]Continenza and G. Profeta, J. Phys. Conf. Ser. **200**, 032014 (2010).